Superalloys 2012: 12th International Symposium on Superalloys
Edited by: Eric S. Huron, Roger C. Reed, Mark C. Hardy, Michael J. Mills, Rick E. Montero, Pedro D. Portella, Jack Telesman
TMS (The Minerals, Metals & Materials Society), 2012

COMPARISON OF THE MECHANICAL BEHAVIOUR AND EVALUATION OF DIFFERENT DAMAGE MECHANISMS IN AN EQUIAXED AND A SINGLE CRYSTAL SUPERALLOYS SUBJECTED TO CREEP, LCF AND TMF

E. Vacchieri[1], A. Costa[1]
[1]Ansaldo Energia S.p.A. 118 Corso Perrone, Genoa, 16161, Italy

Keywords: Ni based superalloys, Creep and Fatigue, Rafting, EBSD, In-Beam detector

Abstract

Hot gas path components in a gas turbine engine for power generation have to withstand to critical conditions in terms of temperature and load distribution. The requirement of higher flexibility of gas turbine engines drives the OEM producer to increase their knowledge of materials behaviour when creep and fatigue coexist. This paper tries to summarise and compare the microstructural damage evolution in two superalloys applied in Ansaldo gas turbine engine components with a different solidification process, René 80 and PWA 1483 SX. The samples from an intensive campaign of mechanical characterisation were used to study damage features after creep, LCF and TMF tests. They have been analysed through standard metallography and advanced characterisation techniques, like EBSD and In-Beam detector in a FEG-SEM. In depth microstructural investigations enabled characterization of damage evolution as a function of testing conditions and highlighted the differences that exist between equiaxed and single crystal alloys. For both the alloys creep-fatigue interaction happens also in presence of compressive hold time LCF and TMF cycles.

Introduction

Ni based superalloys are generally employed in hot gas path components of land gas turbines. The high inlet temperature drives the OEM producer to use more advanced alloys having higher mechanical resistance, in particular creep and microstructural stability, in the service temperature range for the most critical components. Thus for land based turbine engines both polycristalline and single crystal superalloys are employed in the blade and vane applications.

Obviously not only the service temperature ascribes criticality to a component, but its complex geometry, temperature distribution due to internal and film cooling are drivers for fatigue phenomena.

The high flexibility that is demanded by the energy production market, increases the challenge and the coexistence of creep and fatigue should be taken into account in the component design and lifing.

The characterisation of damage in superalloys after laboratory tests, that simulate separately and together the phenomena that happen during actual operation of the turbine, is very important for an OEM because it allows understanding of its evolution and to correlate it to what is observed after service. In fact, creep and fatigue due to the high cycling requirement of the engines can affect each other during a real service life.

Nickel base superalloys have been and still are the most important materials for use in turbine components because of their outstanding high temperature strength. Moreover the development of advanced solidification technologies allows for the widespread application of monocrystalline nickel base superalloys.

The superior strength properties of these alloys come from the combined effect of precipitation hardening by a high volume fraction of the ordered coherently embedded Ni_3Al γ' phase particles and the strong solid solution hardening of the γ matrix. The features of the γ' phase and of this γ/γ' composite microstructure play a fundamental role in the physical metallurgy of superalloys. In fact the great stability of this microstructure at high temperature and under the application of mechanical and thermal loading allows it to reach high temperature material performances [1, 2].

As γ' phase becomes large volume fraction, in particular in the more advanced superalloys, the γ matrix has very narrow channels and for this reason the movements of dislocation are slowed down. Moreover the coherency of γ' phase causes internal stresses that are very important to the microstructural stability and they drive the evolution of these phases during high temperature service exposure. In particular the lattice misfit between γ' phase and γ matrix has been considered as one of the most important microstructural parameters that controls the mechanical properties of superalloys. Usually the lattice misfit is negative and small (around 10^{-3}) in many commercial superalloys, both conventionally cast and single crystal, and it increases with increasing temperature [1, 2].

In this study the main focus has been devoted to the microstructural characterisation of the damage after different laboratory tests that simulate separately and together the main phenomena that occur during service for two Ni based superalloys, one polycrystalline and one single crystal. In particular, apart from classical creep and fatigue tests, some cyclic hold and TMF tests have been performed to reproduce real service conditions at the component critical locations.

The goal of this work is the understanding of damage evolution in the two examined alloys, and also the support to component lifing when this knowledge is applied to the observations made on operated components.

Materials and Methods

The two examined Ni based superalloys are a polycrystalline René 80 and a single crystal PWA 1483 SX. The materials are suitable for component applications operating at high temperatures, and they are employed for vanes and blades in gas turbines.

Table I. Chemical composition (wt%) of the two superalloys.

	Wt%										
Element	Ni	Cr	Co	Al	Ti	W	Mo	Ta	C	Zr	B
René80	Bal.	14.0	9.50	3.00	5.00	4.00	4.00	-	0.17	0.05	0.02
PWA1483SX	Bal.	12.2	9.00	3.60	4.08	3.80	1.90	5.00	0.07	-	-

In Table I their chemical composition is reported. They were analysed after uniaxial creep, LCF and TMF tests.

Mechanical test specimens were machined from investment casting test bars for both the alloys. Single crystal alloy bars have been solidified in ⟨001⟩ nominal orientation. The acceptance limit on θ is the same as set for the real component (0-15°). All the specimens were tested in fully heat treated condition. In Table II the heat treatments plans are reported for both the materials.

The starting microstructure for René 80 is composed of a bimodal distribution of γ' phase; primary particles size is about 400 nm and secondary particles are smaller than 20 nm, with a total volume fraction that reaches about 50%. The differences between the present paper value and what can be found in literature [3, 4] is mainly due to the different heat treatment plan. Due to the relative high temperature of the ageing treatment, the secondary particles are very small and sparse. PWA 1483 SX has a monomodal distribution of γ' phase with particle size of about 500 nm, with a volume fraction of about 60%. In Figure 1 two micrographs depict the microstructure of these two alloys.

Table II. Heat treatment plan for the two superalloys.

Material	Heat Treatment Plan
René 80	1204°C/2h, 1095°C/4h, 1080°C/4h, 870°C/12h
PWA 1483 SX	1260°C/2h, 1080°C/6h

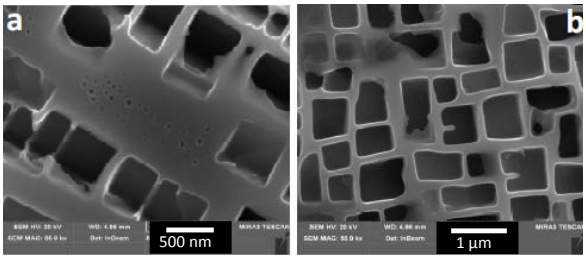

Figure 1. SEM micrographs of the as delivered γ/γ' microstructure for (a) René 80 and (b) PWA 1483 SX.

The creep tests have been conducted for René 80 in the temperature range from 800°C to 950°C, while for the single crystal superalloy the creep test temperatures ranged between 900°C to 1000°C. All the tests, conducted at constant load in air, reached rupture. For both materials the longest test duration was close to 20000 hours.

LCF tests for both the materials have been performed in strain control with a triangular wave, $R(\varepsilon_{min}/\varepsilon_{max}) = -1$ and a constant strain rate of 10^{-2} s^{-1}. Test temperatures for René 80 are 400°C, 800°C and 900°C, while for SX alloy they are 850°C and 950°C. The total strain ranges (from 0.5% to 1.5%) have been chosen for both materials to have a number of cycles to failure up to 10000. All the samples reached failure criteria (20% load drop).

The cyclic hold tests have been conducted at the highest LCF test temperature for Renè80, while for PWA 1483 SX these tests have been performed at both the LCF test temperatures. The dwell time for both the alloys is 20 minutes in the compressive part of the cycle. Also in this case all the samples reached failure criteria (20% load drop).

Finally some TMF tests have been conducted on the studied alloys. The TMF cycle was defined on the basis of the in-service relevant conditions of the metallic coating at the critical location of real components. The main aim was to compare different coatings behaviour. The TMF cycles are essentially Out-of-Phase (OP) cycles, with a hold time in compression at the maximum temperature and a tensile peak during cooling around Ductile-Brittle Transition Temperature (DBTT) of the metallic coatings. The difference between the two materials cycles is the maximum temperature and mechanical strain ranges. All the samples reached failure criteria (20% load drop).

In this paper the main focus has been devoted to the damage evolution estimated through the microstructural investigations on the samples after tests. In particular the longitudinal section of the specimens has been analysed through classical fractographic and metallographic instruments and more advanced characterization techniques, like EBSD and In-Beam detector in a FEG-SEM microscope. EBSD analyses allow evaluating damage through the measurements of misorientation of the collected diffraction patterns with respect to a reference pattern from a damage-free region. In-Beam detector allows for observation of γ/γ' interfacial dislocations as described in literature [5]. For these investigations the samples should be specially prepared: for In-Beam detector imaging the metallographic samples after polishing have been over-etched with $HF+MoO_3$ reagent (selective etching for γ' phas); for EBSD mapping the samples have been prepared adding intermediate etchings after each polishing step and an extra final polishing stage with colloidal SiO_2.

Results and Discussion

The different solidification conditions of the two materials are very important in the evolution of damage after different tests that try to simulate service conditions and to define the material design limits.

In particular the location of damage can be different and moreover the diverse γ' coherent phase distribution greatly affects the alloy mechanical behaviour and damage evolution.

The different damage modes have been analysed separately for the two alloys; then a summary and a comparison between the two alloys' damage evolution mechanisms is reported.

Creep damage

The creep behavior of René 80 alloy is consistent with the bahaviour of high temperature alloys. It doesn't show a steady state at the explored experimental conditions but rather a small decelerating primary stage that is followed by a large and long tertiary regime [6], as depicted in the full-line creep curve of Figure 2. The ductility of the alloy is small and low values of elongation and reduction of area are registered.

PWA 1483 SX creep curves, with applied load along the ⟨001⟩ solidification direction, in the covered temperature/load ranges show the presence of a very small primary stage followed by a steady state that can be quite long, if the applied load is low, and then an accelerating tertiary regime, as shown in Figure 2 (dotted-line curve). In this alloy the elongation and reduction of area to failure reach higher values with respect to the polycrystalline alloy.

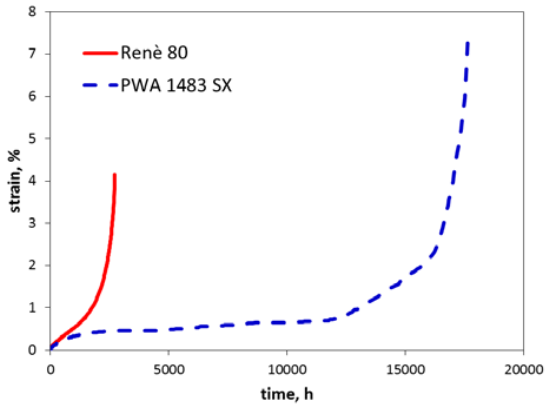

Figure 2. Creep curves of René 80 (full line) and PWA 1483 SX (dotted line) tested to 900°C with the same load.

René 80. The fragile behavior of René 80 is mainly related to the damage localization at the grain boundaries, that are completely absent in the SX material. In fact the presence of the grain boundaries allows intergranular cracks that develop quickly without a huge presence of classical creep damage, like micro-voids and cavitations in these regions (Figure 3-a).

The EBSD map, shown in Figure 4, helps to explain and confirms that the damage is mainly localised in the region near the grain boundaries, where a high misorientation can be measured. This parameter gives an evaluation of the deformation condition of the material with respect to a reference point from an unstrained region [7-9]. Another interesting feature of the EBSD map results is that there is a different damage level in each solidification grain because of their different orientation with respect to the applied load direction. Looking at the internal cracks in more details it has been possible to observe through EBSD analyses that the grain boundary during the test, in particular at the highest temperature, changes its features and is characterised by a continuous layer of γ' phase, surrounded by secondary phases, that is no more coherent with the matrix but it has its own recrystallised grains, with twinning inside, Figure 4-a. The recrystallisation of these small grains can be a preferential damage nucleation as they surely have very poor mechanical properties as γ' phase alone is rather fragile. This observation has been performed also in region far from the cracks and it cannot be ascribed to an oxidation assisted phenomena.

However the creep damage is widespread inside each solidification grain, leading to the modification of γ' phase shape. The N-rafting is present also in this polycrystalline alloy for temperatures higher than 850°C (Figure 3-a). So the lattice misfit should be negative as reported in literature [4, 10 and 11]. The rafted γ' phases are not perfectly normal to the loading direction because each grain has its own random orientation with respect to the loading direction, in contrast to what happens for single crystal alloys. Secondary γ' phase is not observable in all the examined samples and thus at the lowest test temperature it is completely dissolved and merged with primary γ' phase particles during the test.

EBSD maps and In-Beam micrographs help to differentiate between low and high temperature damage (Figure 5-a):

- at low temperature where no rafting happens the microstructure is characterised by the presence of twins with specific orientation with respect to the loading direction and to grain orientation;
- at high temperature the loss of coherence between γ and γ' phase happens in the region under the fracture surface (tertiary regime), as it is possible to observe low angle boundaries that edge and highlight the rafted particles.

PWA 1483 SX. Single crystal alloy shows a widespread damage with a huge amount of internal cracks mainly localised to intradendritic regions (Figure 3-b), that represent the weakest part of the material. Also EBSD maps and γ' phase features highlight the more generalised damage along the longitudinal section, Figure 4-b; in fact the misorientation levels, measured through EBSD maps, are higher with respect to René 80 samples and N-rafting characterises the whole gauge length (Figure 2-b), as expected for a negative γ/γ' misfit superalloy [2, 12]. It has not been possible to observe a difference between low and high temperature creep damage probably because the low temperature is not low enough to hinder high temperature mechanisms; in fact at all the explored temperatures the rafted γ' phase assumes a wavy microstructure towards the fracture surface (rafting regime [1]), that occurs with the loss of coherence, and in some cases even a complete recrystallization, highlighted by EBSD maps. Also In-Beam images confirm EBSD maps, highlighting the loss of coherence of γ/γ' phase and the density of interfacial dislocations; an example is reported for the lowest explored temperature, 900°C, in Figure 5-b.

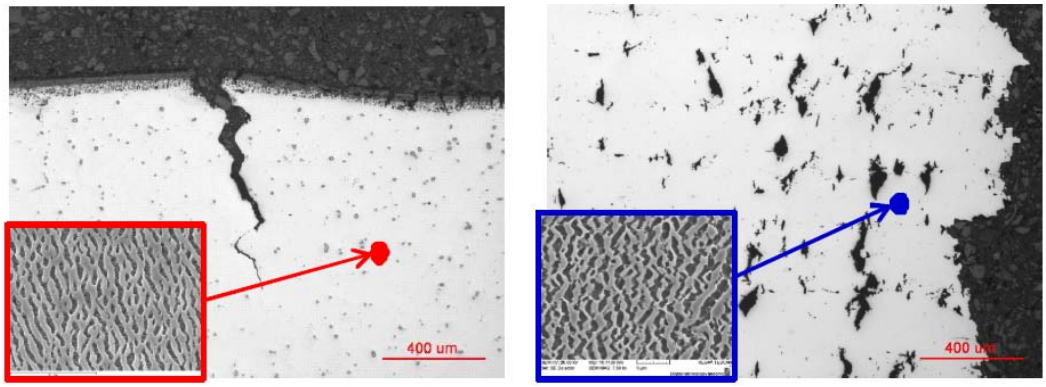

(a) (b)

Figure 3. Creep damage localisation and γ' phase features in (a) René 80 and (b) PWA 1483 SX sample gauge length.

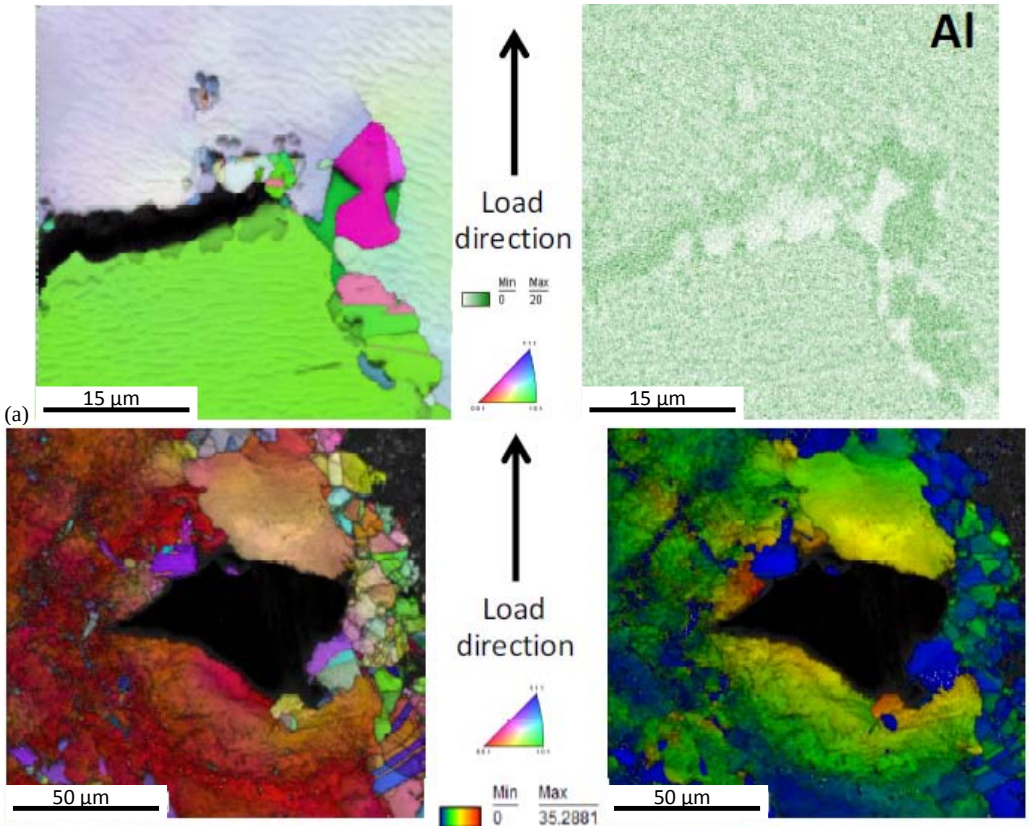

(a)

(b)

Figure 4. EBSD maps at low magnification of creep damage in (a) René 80 and (b) PWA 1483 SX sample gauge length: (a) Inverse Pole Figure +Image Quality (IPF+IQ) map on the left and Al EDS map on the right; (b) Inverse Pole Figure +Image Quality (IPF+IQ) map on the left and Grain Reference Orientation Deviation +Image Quality (GROD+IQ) map on the right, with intensity scale in the centre.

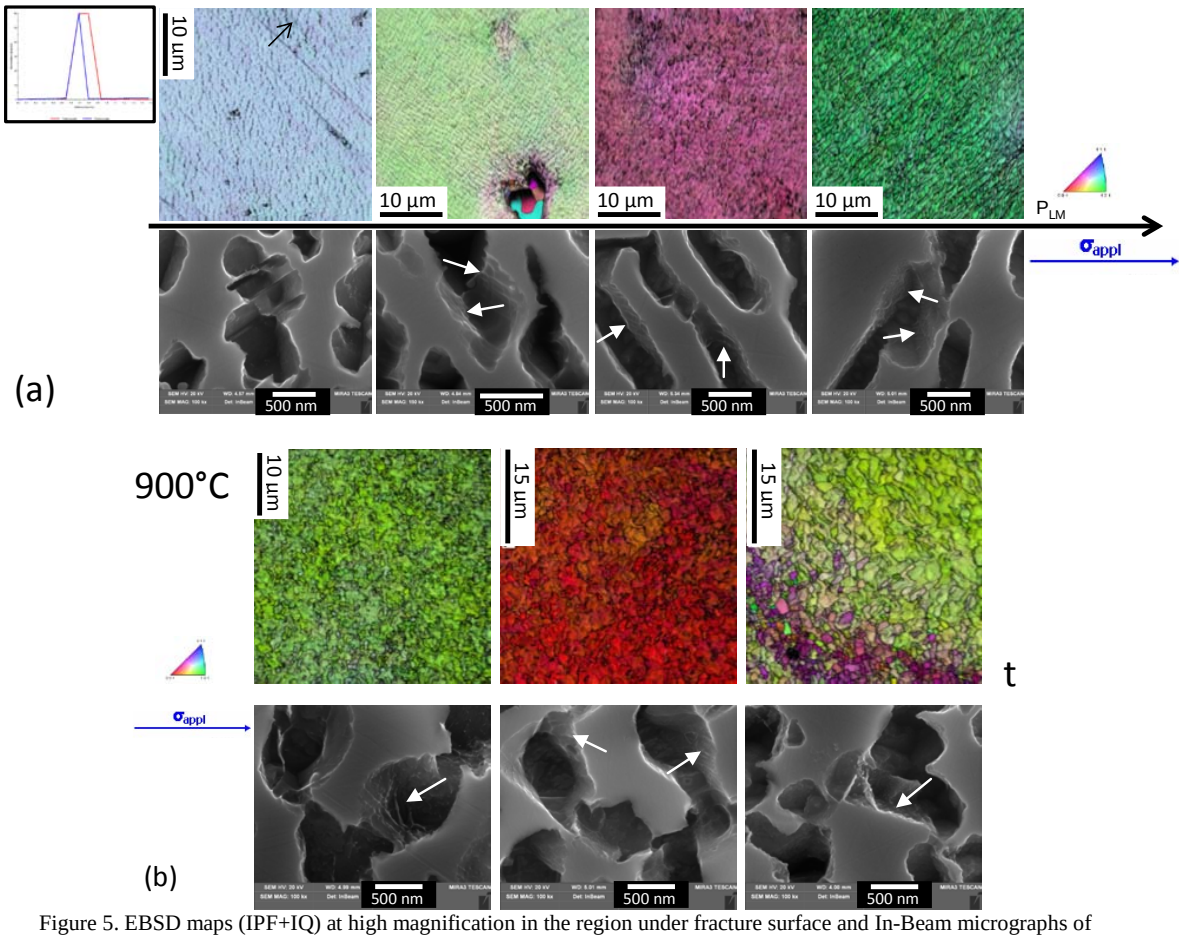

Figure 5. EBSD maps (IPF+IQ) at high magnification in the region under fracture surface and In-Beam micrographs of the γ/γ' microstructure and interfacial dislocations (pointed out by white arrows) from the same regions in (a) René 80 creep samples as a function of Larson-Miller parameter (from left to right 800°C/310MPa, 850°C/250MPa, 900°C/160MPa and 950°C/130MPa) and (b) PWA 1483 SX creep samples tested at 900°C as a function of test duration (from left to right 260MPa, 200MPa and 150MPa).

Fatigue damage

The LCF properties of both the alloys decrease with the increase of temperature and it is particularly evident for the smallest strain ranges. Obviously the single crystal alloy shows a better fatigue resistance than equiaxed alloy, as shown in Figure 6.

René 80. The fracture surfaces are characterised by the presence of secondary crack initiations with small propagation paths and a main crack propagation, that rarely occupied more than the half of the whole fracture surface; these propagation areas are flat albeit it isn't possible to observe the classical fatigue striations, because of the features of this class of alloy and the oxidation phenomena, Figure 7-a. Looking at the lateral surface the presence of very small secondary cracks, normal to the loading direction, that arise from grain boundaries and carbides, is quite limited and it increases slightly with testing temperature, Figure 7-a.

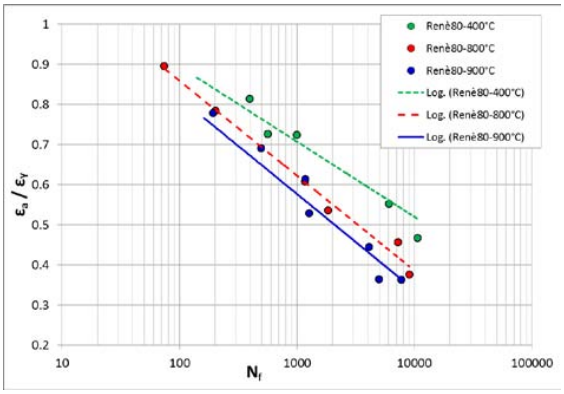

(a)

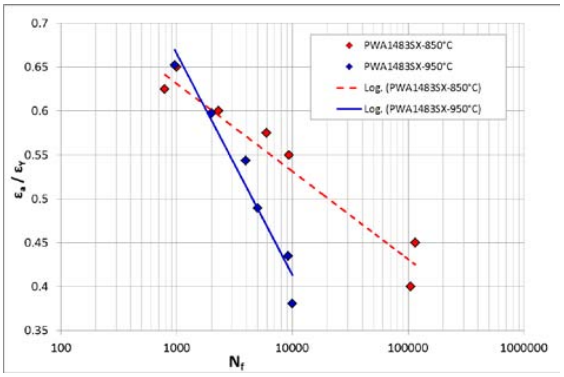

(b)

Figure 6. Comparison of the LCF behavior of the two alloys, (a) René 80 and (b) PWA 1483 SX - ratio between strain amplitude and cyclic yield strain as a function of the number of cycles to failure.

The fractographic analyses have been confirmed through the examination of the longitudinal sections. In fact the presence of secondary cracks is very limited. More detailed analyses on the longitudinal sections allow for a characterization of the fatigue damage in this alloy. In fact EBSD maps show the presence of a highly deformed layer beneath the external surface at all the test temperatures; this area at the highest temperatures is accompanied by a recrystallised layer whose thickness increases with testing duration and temperature, Figure 8. The regions far from the external surface are free of these highly deformed areas. The crack initiation seems to be correlated to the damage accumulation in this region of the samples even if the surface defects are the main source of cracks due to LCF. The recrystallised layer arises from a synergic effect of oxidation and local deformation and it cannot be due to sample machining because it is observed along crack path too. The deformed layer is characterised by the presence of low angle boundary lines that correspond to slip bands that shear γ' phase particles (Figure 9-a); these aspects have been also highlighted through InBeam images that show the γ/γ' phase microstructure and allow to describe the interfacial dislocation, (Figure 9-b). Obviously it is important to add that, even if the cracks are all transgranular and normal to the loading direction, the grain boundaries play an important role in the crack initiation as they represent a surface discontinuity.

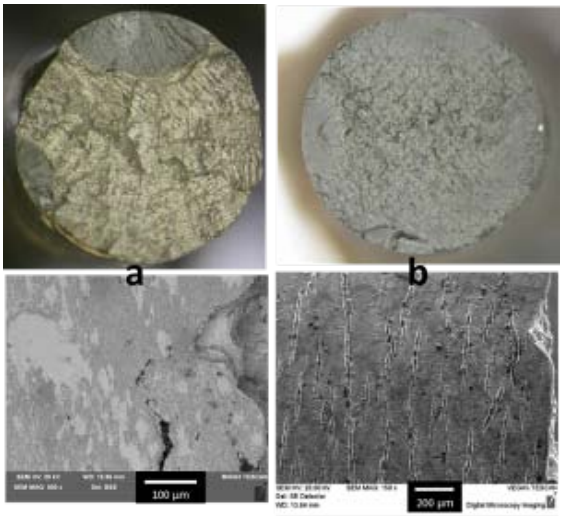

Figure 7. Fracture and external surface of LCF specimens tested at the highest temperature for (a) René 80 and (b) PWA 1483 SX.

PWA 1483 SX. The features of the single crystal alloy samples after LCF have some similarities in the fatigue damage observed in René 80 coupons, even if the absence of grain boundaries is very important in damage development and crack initiation sources. In fact the surface discontinuities in this alloy are mainly the carbides and the intradendritic regions that emerge on the surface. In contrast to René 80, SX alloy features allow for a greater number of crack initiations and propagations on the fracture surface and of secondary cracks along the external surfaces, Figure 7-b. The frequency of the secondary cracks seems to be correlated with the applied strain range: as it increases their frequency decreases, Figure 10. In fact the propagation of the main crack has the upper hand over the other ones increasing the applied strain range. As for creep, the SX alloy seems to be more tolerant to the applied load and to absorb damage before rupture or failure criteria. Looking in more details at the material under external surface, the recrystallised and the deformed layers are present also in PWA 1483 SX (Figure 9) and they are associated with the presence of low angle boundaries and slip bands that shear γ' phase particles, like it has been observed for René 80 (Figure 10).

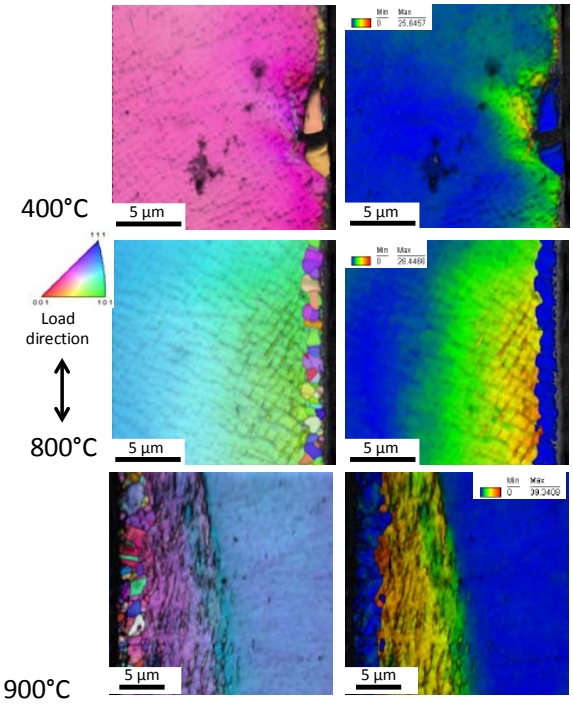

Figure 8. EBSD maps (IPS+IQ on the left and GROD+IQ on the right) under the external surface in René 80 LCF samples that show the deformed region and the presence of a recrystallised layer for the higher temperatures.

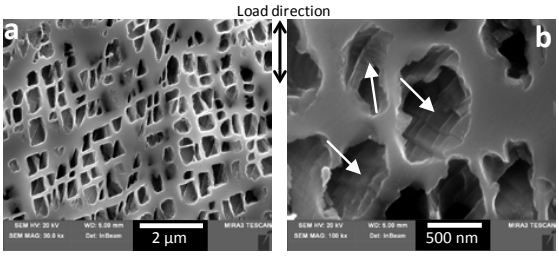

Figure 9. FEG-SEM In-Beam micrographs of the René 80 specimen after LCF test at 900°C: γ/γ' microstructure (a) below the external surface which show slip bands and (b) particular of the γ/γ' interfacial dislocation networks (pointed out by white arrows).

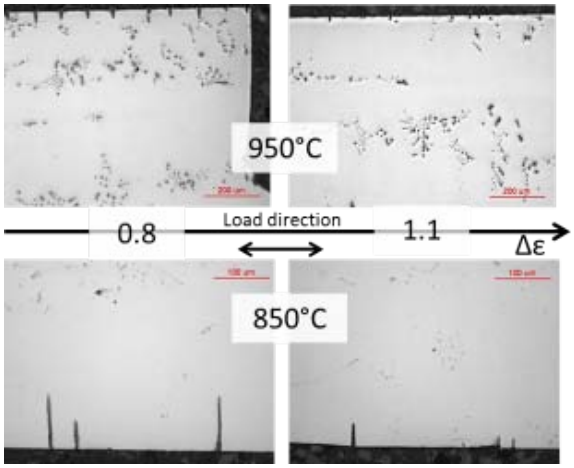

Figure 10. OM micrographs of the longitudinal sections of the SX alloy LCF specimens as a function of applied strain for the two test temperatures.

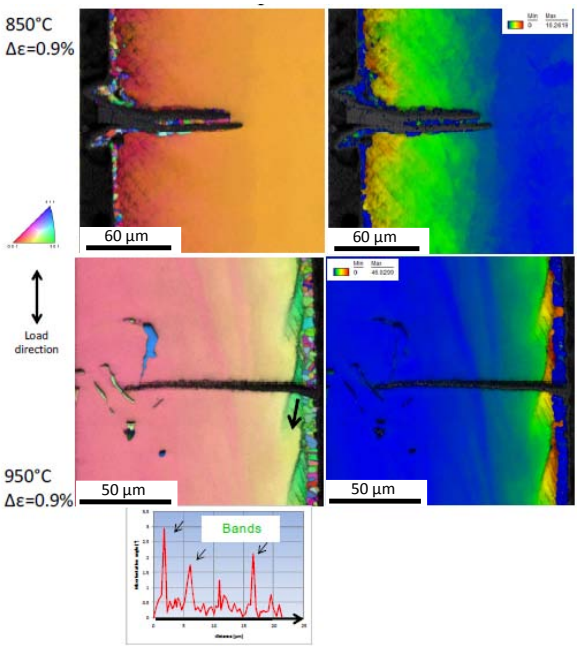

Figure 11. EBSD maps (IPS+IQ on the left and GROD+IQ on the right) under the external surface that depict a secondary crack in PWA 1483 SX LCF samples that highlight the presence of the deformed region with slip bands and the recrystallised layer.

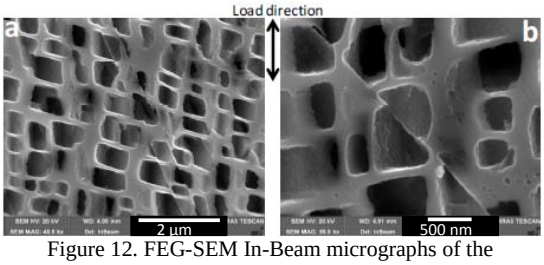

Figure 12. FEG-SEM In-Beam micrographs of the SX alloy specimen after LCF test at 850°C: γ/γ' microstructure (a) underneath the external surface and (b) sheared γ' phase particle.

Creep-fatigue damage

The interaction of creep and fatigue damage has been examined looking at the samples after hold time LCF tests and after TMF tests. In both cases, hold time and high temperature dwell, correspond to compressive strain.

The effect of hold time in LCF tests and the TMF tests causes a decrease of fatigue endurance for both alloys, as depicted in Figure 13.

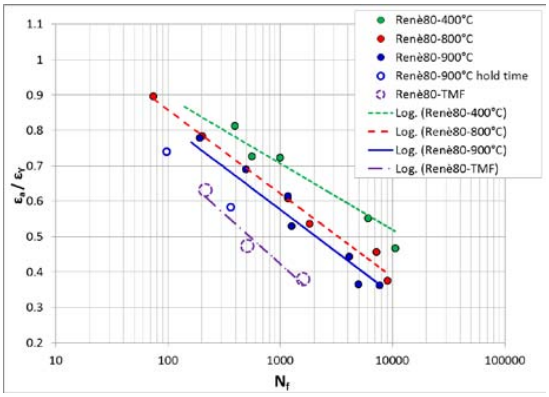

(a)

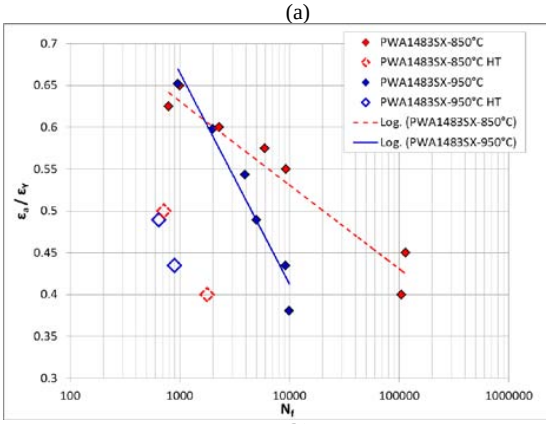

(b)

Figure 13. Cyclic hold and TMF tests results compared with the standard LCF for (a) René 80 and (b) PWA 1483 SX - ratio between strain amplitude and cyclic yield strain as a function of the number of cycles to failure.

René 80. The compressive hold time at the highest test temperature for René 80 brings on a great number of secondary cracks along the external surface of the samples. Looking at the microstructural features the hold time creates a thicker oxide scale that is very fragile, so it cracks easily and acts as a preferential crack initiation site for the fatigue damage, Figure 14-a. In TMF specimens some cracks initiate and propagate along the grain boundaries, then they continue to propagate transgranularly normal to the loading direction, Figure 14-b.

The reduction of endurance after these tests should be ascribed to the oxide scale growth even if some creep damages have been observed in the samples. In fact γ/γ' phase microstructure is affected by these tests as a huge amount of disordered interfacial dislocations networks has been observed; moreover some grain boundary recrystallisation phenomena and twins can be detected in the samples. This damage is mainly localised under the external surface but with respect to the LCF specimens it have been found also far from the more damaged regions, Figure 15.

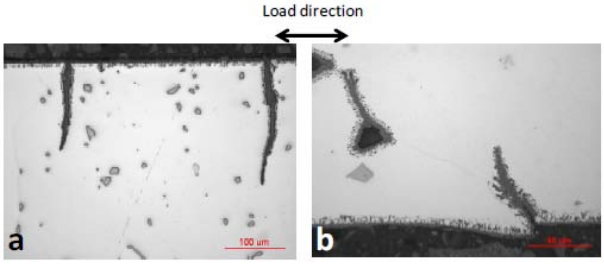

Figure 14. OM micrographs from René 80 (a) HT-LCF specimen and (b) TMF coupon [13].

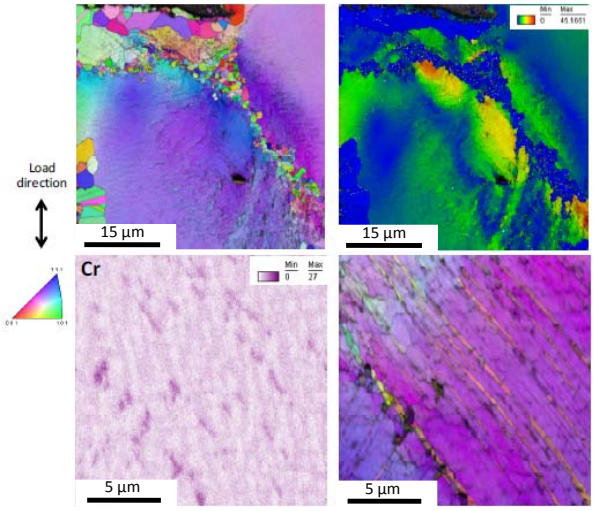

Figure 15. EBSD maps of René 80 TMF sample: (a) IPF+IQ and GROD+IQ particular of a region near the external surface under a secondary crack that show the presence of recrystallisation along the grain boundary; (b) Cr EDS map and IPF+IQ particular of the microstructure in an internal grain which show presence of twins and precipitation of secondary phases highlighted by Cr EDS map distribution.

PWA 1483 SX. The cyclic hold tests, isothermal and non-isothermal, for SX alloys have developed a slightly bigger amount of secondary cracks, related to a thicker oxide scale and recrystallised layer, with respect to the classical LCF specimens. As for René 80, the reduction of fatigue endurance can be ascribed mainly to oxide behaviour in crack initiation but signs of creep damage have been observed. γ/γ' phase microstructure shows the presence of a starting P-rafting, due to the compressive hold in a negative γ/γ misfit alloy [2, 12], and of organised arrangements of γ/γ' interfacial dislocations (Figure 16). Moreover the presence of small area of recrystallisation around carbides and intradendritic regions starts to appear in the more damaged region, near the fracture surface, Figure 17.

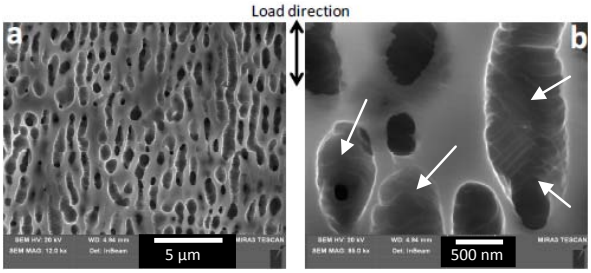

Figure 16. FEG-SEM In-Beam micrographs of a PWA 1483 SX TMF sample: (a) P-rafting in the region near the fracture surface and near the external one; (b) particular of γ/γ' phase interfacial dislocation network pointed out by white arrows).

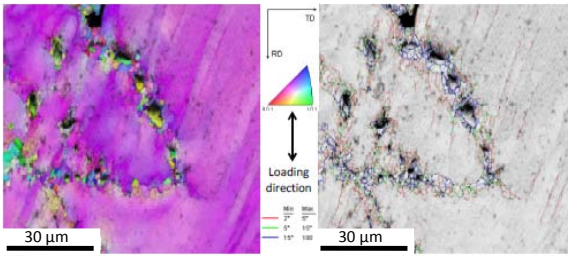

(a) (b)

Figure 17. EBSD maps of PWA 1483 SX TMF specimen (a) IPF+IQ and (b) IQ+GB [13].

Summary of damage features in the two alloys

The damage features after different experimental tests for the two analysed superalloys are compared and summarised.

Creep. The presence of the grain boundaries in the polycrystalline alloy is very important in the damage development. In fact for both the materials, N-rafting has been observed for temperatures over 850°C but, for SX material, the modification of γ/γ' features is widespread in the alloy microstructure. The γ/γ' microstructure modification leads to the loss of coherence between these phases and it can be experimentally valued through the presence of low angle boundaries between them (detected by EBSD maps, see Figure 5), particularly in the more damaged regions near the fracture surface. For René 80, the damage is localized at the grain boundaries and in some grains with a preferential orientation in relation to the loading direction. Moreover the low temperature creep damage behaviour for the polycrystalline alloy has been verified through EBSD maps and In-Beam images, as twins and shearing of γ' phase particle have been observed, see Figure 5-a. For the equiaxed alloy, secondary γ' phase effect on microstructural creep damage has not been evaluated as in all the examined samples it was completely dissolved and merged with primary γ' phase particles.

Fatigue. The fatigue damage for the two alloys is quite similar in term of its localisation and features. Grain boundaries in polycrystalline alloy have a minor role in damage development. In fact, even if they act as crack initiation sources, secondary cracks have been rarely observed in these samples. When a crack starts, the crack tends to propagate quite quickly reaching the failure criteria of the test, hindering the nucleation of several secondary cracks along the gauge length within the test duration. This is true for all the explored strain ranges and temperatures. SX material seems to absorb more of the fatigue damage as multiple crack initiation is more common on the fracture surface and several secondary cracks can be observed along the sample gauge length at both the temperatures. The frequency of secondary cracks diminishes with the increase of strain range as the main crack propagation increases.

Creep-fatigue. When creep and fatigue interact in the two materials, they affect the endurance of the test even if a key role in the reduction of life is played by oxidation. In fact, the oxide layer is fragile and during compressive hold it cracks and creates several crack initiation sites. In fact, René 80 samples after cyclic hold tests or TMF tests show the presence of secondary cracks that have not been observed in LCF coupons. Obviously the compressive creep causes in both the materials some changes in the microstructure that can affect the fatigue resistance of the alloys. In particular, for the equiaxed alloy the presence of recrystallisation along the grain boundaries (see Figure 15) is similar to the damage observed in the crept specimen (see Figure 4-a). In the SX specimens the presence of P-rafting and local recrystallisation around carbides and intradendritic regions are in agreement with the development of creep damage after a compressive loading.

The compressive creep damage can affect the fatigue behaviour as the presence of weaker grain boundaries and twins in the alloy microstructure for René 80, and recrystallised regions with loss of coherence between γ and γ' phase can help crack initiation and propagation.

The presence of P-rafting together with organised structures of γ/γ' phase interfacial dislocations (Figure 16) can have a beneficial effect as the increase of dislocation density can hinder the movement of mobile dislocations and slow down the nucleation of slip bands or twins [14, 15] and this can justify the absence of twins in the SX alloy, where more organised interfacial dislocation structures have been observed, rather than in René 80 specimens.

In the present work twins have been found in the equiaxed alloy. In literature some examples have been reported of single crystal Ni based superalloys when subjected to compressive load along ⟨001⟩ direction [14, 16]. These twins can cause stress concentration at the sample surface or inside the material, as extra interfacial boundaries. For this reason, their role in damage evolution during test where creep and fatigue coexist seems to be more damaging in comparison to the slip bands [17].

Some old papers that deal with René 80, that exclude the classical ideas of interaction between creep and fatigue, have ascribed the reduction of fatigue life on aged material to a boundary embrittlement in the near surface regions [10, 18]; this observation has been partially confirmed by the present study even if this damage at the grain boundaries, together with twins nucleation due to not organised interfacial dislocation structures, can be considered a creep damage that interact negatively with the fatigue damage.

All this discussion is based on qualitative microstructural observations of the available specimens, which are all tested until rupture or to failure criteria. Some more quantitative analyses like TEM or neutron diffraction should be done to confirm all the EBSD and In-Beam observations.

Work is on-going on interrupted creep specimens to evaluate the creep damage evolution. Moreover in the future interrupted samples after fatigue and creep-fatigue tests will be performed. A confirmation of EBSD and In-Beam results will be done through quantitative TEM analyses that should allow studying dislocation arrangements during damages' accumulation.

Conclusions

In the present paper the microstructural damage of two Ni based superalloys after different solidification processes has been analysed. A conventionally cast and a single crystal alloys have been compared after creep, fatigue and cyclic hold and TMF tests. The following points sum up the paper results:

- Creep damage is greatly affected by the presence of grain boundaries in the conventionally cast alloy, even if a similar evolution of the microstructure has been observed, in particular for the highest temperatures, with the presence of N-rafting in both materials and loss of coherence between γ and γ' phase in the region near the fracture surface.
- Fatigue damage is slightly affected by the different solidification process even if conventionally cast alloy seems to absorb a low level of deformation before rupture with respect to SX material as a lower number of secondary cracks are observed. The damage develops mainly in the region underneath the external surface which is characterised by the presence of a recrystallised layer due to oxidation/applied load synergic effect and by a highly deformed layer where slip bands, that shear γ' phase particles, appear.
- Creep-fatigue tests with compressive hold time result in a coexistence of creep and fatigue damages. They can have effect on each other due to a reduction of endurance that has been observed for both materials. A further influence that should be considered in the reduction of life is the presence of a thicker and fragile oxide layer that characterises the specimens of both the alloys.

In the future some further exams of interrupted tests and some quantitative analyses by TEM will be performed in order to validate the obtained results.

References

1. R.C. Reed, *The superalloys, fundamentals and applications* (Cambridge, Cambridge University Press, 2006) 33-120, 121-216.
2. H. Mughrabi, "Microstructural aspects of high temperature deformation of monocrystalline nickel base superalloys: some open problems", Materials Science and Technology 25 (2) (2009) 191-204.
3. J. Safari, S. Nategh, "On the heat treatment of Rene-80 nickel-base superalloy", Journal of Materials Processing Technology 176 (2006) 240–250.
4. J. Safari, S. Nategh, "Low cycle fatigue mechanism of Rene´ 80 at high temperature–high strain ", Materials Science and Engineering A 494 (2008) 385–390.
5. A. Epishin, "SEM investigation of interfacial dislocations in nickel-base superalloys", Journal of Microscopy 228 (2) (2007) 110–117.
6. V. Lupinc et al., "Creep curve modelling of a conventionally cast Nickel base superalloy", Proceedings of 9th Liège Conference on Materials for Advanced Power Engineering, Liège 25th – 27th September 2010.
7. Rika Yodaa, Toshinori Yokomaku, Nobuhiro Tsuji, "Plastic deformation and creep damage evaluations of type 316 austenitic stainless steels by EBSD", Materials Characterization 61 (2010) 913-922.
8. Masayuki Kamayaa, A.J. Wilkinson, J.M. Titchmarsh, "Measurement of plastic strain of polycrystalline material by electron backscatter diffraction", Nuclear Engineering and Design 235 (2005) 713–725.
9. Masayuki Kamayaa, A.J. Wilkinson, J.M. Titchmarsh, "Quantification of plastic strain of stainless steel and nickel alloy by electron backscatter diffraction" Acta Materialia 54 (2006) 539–548.
10. S. D. Antolovich, P. Domas, J. L. Strudel, "Low Cycle Fatigue of Rene 80 as Affected by Prior Exposure", Metallurgical Transaction A 10 (1979) 1859-1868.
11. H.J. Kolkman, "Creep, Fatigue and their Interaction in Coated and Uncoated René 80", Materials Science and Engineering, 89 (1987) 81-91.
12. F.R.N. Nabarro, "Rafting in Superalloys", Metallurgical Transaction A 27 (1996) 513-530.
13. E.Vacchieri, E. Poggio, S. Corcoruto, "Microstructural Degradation of a Cast Ni-based Superalloy after Creep, LCF and TMF Tests", ECCC Creep Conference, 21–23 April 2009, Zurich.
14. E. Vacchieri et al., "Effect of NiCoCrAlYzRe coatings on TMF behaviour of first and second generation single crystal Ni based superalloys", Enery Materials 4 (4) (2012) 197-205.
15. T.P. Gabb, G. Welsch, "The high temperature deformation in cyclic loading of a single crystal nickel-base superalloy", Acta Metallurgica 37 9 (1989) 2507-2516.
16. K. Kakehi, "Tension/compression asymmetry in creep behaviour of a Ni-based superalloy", Scripta Materialia 41 5 (1999) 461-465.
17. J.X. Zhang et al., "Deformation twins and failure due to thermo-mechanical cycling in TMS-75 superalloy", Scripta Materialia 54 (2006) 655-660.
18. S. D. Antolovich, S. Liu, R. Baur, "Low Cycle Fatigue Bahaviour of René 80 at Elevated Temperature", Metallurgical Transaction A 12 (1981) 473-481